Inorg. Chem. **2002**, *41*, 1739–1746

Bonding Behavior of $Co(CO)_3L$ (L = CO, PPh_3) Building Blocks in Platinum–Cobalt Carbonyl Clusters

Robert Bender,*,† Pierre Braunstein,*,† Salah-Eddine Bouaoud,‡ Djamil Rouag,†,‡ Pierre D. Harvey,§ Stéphane Golhen,|| and Lahcène Ouahab||

Laboratoire de Chimie de Coordination, UMR 7513 CNRS, Institut Le Bel, Université Louis Pasteur, 4 rue Blaise Pascal, F-67070 Strasbourg Cedex, France, Institut de Chimie, Université de Constantine, route de Aïn el Bey, Constantine, Algeria, Université de Sherbrooke, Sherbrooke, PQ, Canada, J1K 2R1, and Laboratoire de Chimie du Solide et Inorganique Moléculaire, UMR 6511 CNRS, Institut de Chimie, Université de Rennes 1, Campus de Beaulieu, 35042 Rennes Cedex, France

Received July 11, 2001

The reaction of $[Co(CO)_4]^-$ with $[Pt_2Cl(\mu\text{-}PPh_2)(PPh_3)_3]$ (1:1 ratio), which was prepared in situ by reaction of aqueous HCl with the orthometalated complex $[Pt_2(\mu\text{-}PPh_2)(\mu\text{-}o\text{-}C_6H_4PPh_2)(PPh_3)_2]$, afforded the deep green triangular cluster $[Pt_2Co(\mu\text{-}PPh_2)(CO)_4(PPh_3)_2]$, **7**. X-ray crystallographic analysis reveals that this new cluster contains two formally monoanionic fragments, PPh_2^- and $Co(CO)_4^-$, that bridge a d^9–d^9 Pt(I)–Pt(I) metal–metal bond. Whereas tetracarbonylcobaltate is generally bonded to only one metal center as a 2e donor ligand, it is best viewed here as a formally 4e donor anionic metalloligand. This model leads then to the usual 16e count for each Pt center and relates this metalloligand to other anionic bridging ligands, such as PPh_2^-. A comparative EHMO bonding analysis of $[Co(CO)_3L]^-$ (L = CO, PR_3) fragments is presented which takes into account the possible coordination geometries about cobalt, trigonal bipyramidal (with C_{3v} local symmetry) or edge-capped tetrahedral when referring to the ligand polyhedron (with C_{2v} or C_s symmetry). The results support the description of this unusual bridging bonding mode.

Introduction

Since the early days of heterometallic complexes and clusters containing palladium or platinum, the nucleophilic substitution of halogen atoms on Pd(II) or Pt(II) mononuclear complexes for carbonylmetalate anions has allowed the synthesis of numerous heterometallic complexes which display a wide range of structural types and compositions.[1−5] In general, the metal carbonyl fragment behaves as a terminally bound metalloligand, thus acting as a neutral 1e donor, similar to the halogen ligand it replaces (alternatively, the carbonylmetalate *anion* behaves as a 2e anionic donor ligand, equivalent to a chloride *anion*). This is the case, for example, in *trans*-$[Pt\{Co(CO)_4\}_2L_2]$,[6,7] *trans*-$[Pt\{Fe(CO)_3NO\}_2L_2]$,[7,8] *trans*-$[Pt\{Mn(CO)_5\}_2L_2]$,[7,9] or *trans*-$[Pt\{Mo(\eta\text{-}C_5H_5)(CO)_3\}_2L_2]$ (Scheme 1).[6,7,10]

When the fragment $[Co(CO)_3L]$ (L = CO, PPh_3) binds to a metal center, it generally adopts either of two main geometries. In **1**, the coordination geometry about cobalt is trigonal bipyramidal (with C_{3v} local symmetry), whereas, in **2**, it is of the edge-capped tetrahedral type when referring to the carbonyl polyhedron (with C_{2v} or C_s symmetry).

Reactions of the carbonylmetalates with the Pt(II) or Pd(II) precursor complexes may occur with partial reduction

* Authors to whom correspondence should be addressed. E-mail: braunst@chimie.u-strasbg.fr (P.B.).
† ULP Strasbourg.
‡ Université de Constantine.
§ Université de Sherbrooke.
|| Université de Rennes 1.

(1) Farrugia, L. J. *Adv. Organomet. Chem.* **1990**, *31*, 301.
(2) Braunstein, P. *New J. Chem.* **1994**, *18*, 51.
(3) Adams, R. D. *Comprehensive Organometallic Chemistry II*; Abel, E. W., Stone, F. G. A., Wilkinson, G., Eds.; Pergamon: Oxford, 1995; Vol. 10, p 1.
(4) Chetcuti, M. J. *Comprehensive Organometallic Chemistry II*; Abel, E. W., Stone, F. G. A., Wilkinson, G., Eds.; Pergamon: Oxford, 1995; Vol. 10, p 23.
(5) Farrugia, L. J. *Comprehensive Organometallic Chemistry II*; Abel, E. W., Stone, F. G. A., Wilkinson, G., Eds.; Pergamon: Oxford, 1995; Vol. 10, p 187.
(6) Braunstein, P.; Dehand, J. *Bull. Soc. Chim. Fr.* **1975**, 1997.
(7) Barbier, J. P.; Braunstein, P. *J. Chem. Research, Synop.* **1978**, 412.
(8) Braunstein, P.; Predieri, G.; Lahoz, F. J.; Tiripicchio, A. *J. Organomet. Chem.* **1985**, *288*, C13.
(9) Bars, O.; Braunstein, P.; Jud, J.-M. *New J. Chem.* **1984**, *8*, 771.
(10) Bender, R.; Braunstein, P.; Jud, J.-M.; Dusausoy, Y. *Inorg. Chem.* **1984**, *23*, 4489.

10.1021/ic010739p CCC: $22.00
Published on Web 03/05/2002

Scheme 1

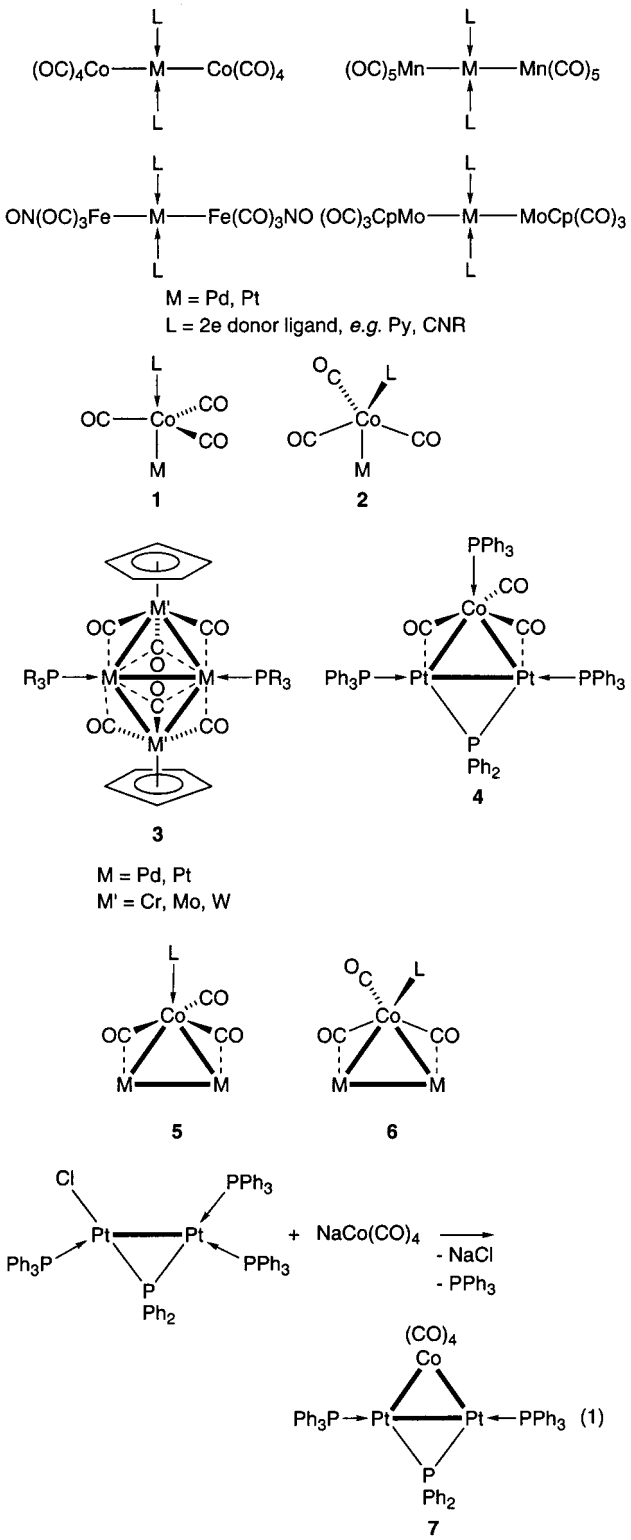

of the metal centers to Pt(I) or Pd(I), respectively. This often results in the formation of a L−M−M−L moiety (M = Pd, Pt), whose M−M bond is bridged by one or two carbonylmetalates behaving as 4e donors. This was first observed in reactions of $[MCl_2(PR_3)_2]$ (M = Pd, Pt) with the $[M'(\eta\text{-}C_5H_5)(CO)_3]^-$ anions (M′ = Cr, Mo, W) which afforded a family of planar, 58e, triangulated tetranuclear $M_2M'_2$ clusters of type **3**.[10−12]

Reaction of $[PtCl_2(PPh_3)_2]$ with 2 equiv of $[Co(CO)_4]^-$ also led to a 58 electron cluster, $[Pt_2Co_2(CO)_8(PPh_3)_2]$, but it has a butterfly structure with a Co−Co hinge and a long Pt···Pt separation of 2.987(4) Å.[13,14] Its controlled thermolysis afforded the trinuclear cluster $[Pt_2Co(\mu\text{-}PPh_2)(CO)_3(PPh_3)_3]$ **4**, which contains a $Ph_3P-Pt-Pt-PPh_3$ fragment bridged by a PPh_2 group and a trigonal pyramidal $Co(CO)_3(PPh_3)$ moiety arranged in such a way to generate a planar $Pt_2Co(\mu\text{-}P)$ core.[15]

When the fragment $Co(CO)_3L$ (L = CO, PPh_3) interacts with *two* metal centers, at least two possible coordination geometries about the cobalt center may be envisaged. They are of trigonal pyramidal (**5**) or tetrahedral geometry (**6**) and derive from **1** and **2**, respectively.

We wondered whether the ligand arrangement adopted by the cobalt moiety in **4** was due to the steric bulk of the apical PPh_3 ligand or corresponds to an intrinsic preference for a bonding mode of type **5** over type **6**. We have now obtained a new cluster, $[Pt_2Co(\mu\text{-}PPh_2)(CO)_4(PPh_3)_2]$, **7**, which differs from **4** by the presence of a distorted tetrahedral $Co(CO)_4$ group instead of a trigonal pyramidal $Co(CO)_3(PPh_3)$ group. We shall see that this has significant structural consequences. We describe the synthesis and characterization by IR and $^{31}P\{^1H\}$ NMR spectroscopy and X-ray diffraction of this new cluster and provide a comparative EHMO study of clusters **4** and **7**.

Experimental Section

All experiments were performed under an inert atmosphere of deoxygenated and dried nitrogen with the use of standard Schlenk techniques. The complex $[Pt_2(\mu\text{-}o\text{-}C_6H_4PPh_2)(\mu\text{-}PPh_2)(PPh_3)_2]$ was synthesized as described in the literature.[16] All solvents were dried and distilled under nitrogen prior to use. Infrared spectra were measured in KBr pellets on a Nicolet 210 FT-IR spectrometer, and NMR spectra, on Bruker MSL 300 (^{31}P at 121.505 MHz). Phosphorus chemical shifts were externally referenced to 85% H_3PO_4 in H_2O, with downfield chemical shifts reported as positive. FAB mass spectra were carried out using a VG ZAB-HF mass spectrometer, in an NBA matrix.

Synthesis of $[Pt_2Co(\mu\text{-}PPh_2)(CO)_4(PPh_3)_2]\cdot 2C_6H_5CH_3$ (7·2PhMe). First, the complex $[Pt_2Cl(\mu\text{-}PPh_2)(PPh_3)_3]$ was prepared in situ by addition of aqueous 0.1 N HCl (1.10 mL, 0.11 mmol) to a solution of $[Pt_2(\mu\text{-}PPh_2)(\mu\text{-}o\text{-}C_6H_4PPh_2)(PPh_3)_2]$ (0.150 g, 0.11 mmol) in THF (50 mL). After the reaction mixture was stirred for 20 min, a solution of $Na[Co(CO)_4]$ (4.8 mL, 0.112 mmol), prepared by reduction of $[Co_2(CO)_8]$ (0.400 g) in THF (100 mL) over a 5% sodium amalgam, was then added. The yellow solution turned deep green. After further stirring for 2 h at room temperature, the solvent was evaporated to dryness under reduced pressure, and the green residue was washed with hexane and dried under vacuum. After

(11) Bender, R.; Braunstein, P.; Dusausoy, Y.; Protas, J. *Angew. Chem., Int. Ed. Engl.* **1978**, *17*, 596.
(12) Bender, R.; Braunstein, P.; Jud, J.-M.; Dusausoy, Y. *Inorg. Chem.* **1983**, *22*, 3394.
(13) Fischer, J.; Mitschler, A.; Weiss, R.; Dehand, J.; Nennig, J.-F. *J. Organomet. Chem.* **1975**, *91*, C37.
(14) Braunstein, P.; Dehand, J.; Nennig, J.-F. *J. Organomet. Chem.* **1975**, *92*, 117.
(15) Bender, R.; Braunstein, P.; Metz, B.; Lemoine, P. *Organometallics* **1984**, *3*, 381.
(16) Bender, R.; Bouaoud, S.-E.; Braunstein, P.; Dusausoy, Y.; Merabet, N.; Raya, J.; Rouag, D. *J. Chem. Soc., Dalton Trans.* **1999**, 735.

Table 1. Crystal Data and Structure Refinement for Compound $[Pt_2Co(\mu\text{-}PPh_2)(CO)_4(PPh_3)_2]\cdot 2C_6H_5CH_3$ (**7**·2PhMe)

chemical formula	$C_{66}H_{56}O_4P_3Pt_2Co$
fw	1455.13
T/K	233(2)
cryst syst	triclinic
space group	$P\bar{1}$
a/Å	11.791(4)
b/Å	13.471(6)
c/Å	18.887(9)
α/deg	106.654(4)
β/deg	95.844(3)
γ/deg	92.983(4)
V/Å^3	2849(2)
ρ(calc)/ g·cm^{-3}	1.696
Z	2
μ/mm^{-1}	5.319
reflns collected/unique	10562/10028
R(int)	0.0361
R1 [$I > 2\sigma(I)$][a]	0.0444
wR2 [$I > 2\sigma(I)$][b]	0.1040

[a] $R1 = \sum||F_o| - |F_c||/\sum|F_o|$. [b] $wR2 = \{\sum[w(F_o^2 - F_c^2)^2]/\sum[w(F_o^2)^2]\}^{1/2}$.

dissolution in toluene and addition of hexane, **7**·2PhMe (0.120 g, yield: 73%) crystallized out as green crystals, suitable for X-ray diffraction. Anal. Calcd for $C_{66}H_{56}O_4CoP_3Pt_2$ (M = 1455.21): C, 54.48; H, 3.88. Found: C, 53.80; H, 4.01. IR (KBr) ν(CO): 2002-(vs), 1954 (vs), 1860(s), 1795 (vs). $^{31}P\{^1H\}$ NMR: δ 41.1 [d, PPh_3, ^2J(P−P) 26 Hz, ^1J(P−Pt) 4380 Hz, ^2J(P−Pt) 112 Hz, ^3J(P−P) 87 Hz], 208.5 [t, μ-P, ^2J(P−P) 26 Hz, ^1J(P−Pt) 2608 Hz]. Mass spectrum (intensity in %): *m*/*z* 1214 [M − 2CO, 20%]$^+$, 1186 [M − 3CO, 15%]$^+$, 1158 [M − 4CO, 100%]$^+$, 1099 [M − $Co(CO)_4$, 53%]$^+$.

Crystallographic Data Collection and Structure Determination. Single crystals were mounted on an Enraf-Nonius CAD4 diffractometer equipped with a graphite monochromated Mo Kα radiation source (λ = 0.71073 Å). Cell dimensions and orientation matrix for data collection were obtained from least-squares refinement, using the setting angles of 25 centered reflections. The crystal data are summarized in Table 1. The intensities were collected (θ−2θ scans) at 233 K; no significant decay was observed in the three standard reflections measured every hour during data collection. Data reduction and correction were performed with MolEN.[17] Lorentz polarizations and semiempirical absorption corrections (ψ-scan method)[18] were applied to intensities for all data. Scattering factors and corrections for anomalous dispersion were taken from the literature.[19] The structure was solved with SHELXS-97[20] and refined with SHELXL-97 programs by full matrix least-squares method, on F^2. All non-hydrogen atoms were refined anisotropically, while hydrogen atoms were assigned an isotropic thermal parameter 1.2 times that of the parent atom (1.5 for terminal atoms) and allowed to ride.

Computational Details. All the EHMO calculations were of the extended Huckel type (EHMO)[21−23] using a modified version of the Wolfsberg−Helmholz formula.[24] The atomic parameters for C,[21,23] O,[21,23] P,[25] H,[21,23] Pt,[26] and Co[26] were taken from the literature. Because of the limitations in the size of molecules handled by the program, PPh_3 was replaced by PH_3. This is a standard methodology.[27] Hence, the computed molecule was $[Pt_2Co(\mu\text{-}PH_2)(PH_3)_2(\mu\text{-}CO)_2(CO)_2]$. The bond distances and angles are those reported in the X-ray structure (average values). For the $[Co(CO)_4]^-$ anion in the T_d, C_{2v}, C_{3v}, and C_s symmetries, all distances were kept constant and averaged using the X-ray data as well.

Results

The reaction of $[Co(CO)_4]^-$ with $[Pt_2Cl(\mu\text{-}PPh_2)(PPh_3)_3]$[28] (1:1 ratio), which was prepared *in situ* by attack of HCl on the orthometalated complex $[Pt_2(\mu\text{-}PPh_2)(\mu\text{-}o\text{-}C_6H_4PPh_2)(PPh_3)_2]$,[16] afforded the deep green cluster $[Pt_2Co(\mu\text{-}PPh_2)(CO)_4(PPh_3)_2]$, **7** (eq 1).

The mass spectrum of **7** does not contain the molecular peak $[M]^+$, but fragments resulting from stepwise loss of carbonyl ligands at *m*/*z* = $[M - 2CO]^+$, $[M - 3CO]^+$, $[M - 4CO]^+$, and $[M - Co(CO)_4]^+$. Its IR spectrum (KBr) presents two high and two low frequency ν(CO) absorption bands at 2002(vs), 1954 (vs), 1860(s), 1795 (vs) cm^{-1}, which are indicative of two terminal and two bridging carbonyls, respectively. The $^{31}P\{^1H\}$ NMR spectrum shows a doublet and a triplet, flanked each by satellites due to ^1J(P−Pt) and ^2J(P−Pt) couplings. The triplet at low field is assigned to the P atom bridging two equivalent Pt atoms. The doublet at 41.1 ppm is due to the terminal phosphines, and the pattern of the satellites is that of a P−Pt−Pt−P chain, similar to that found in other complexes containing this unit.[10] These data are fully consistent with the structure found in the solid state.

X-ray Structure of $[Pt_2Co(\mu\text{-}PPh_2)(CO)_4(PPh_3)_2]\cdot 2PhMe$ (7·2 PhMe). A view of molecule **7** is shown in Figure 1, and selected bond distances and angles are given in Table 2. The cluster crystallizes with two molecules of toluene. The metallic core of this molecule is formed by a Pt_2Co triangle, whose intermetallic distances, d(Pt−Co) = 2.547-(2) and 2.574(2) Å, and d(Pt−Pt) = 2.655(1) Å, are in the range found in other Pt−Co clusters.[1,14,29] Each Pt atom bears a PPh_3 ligand, and the P−Pt−Pt−P chain is almost linear. The Pt−Pt bond is doubly bridged, symmetrically by a PPh_2 group and a $Co(CO)_4$ moiety, in such a way that the Pt, Co, and μ-P atoms are coplanar. The coordination geometry about the Co atom is defined by two terminal carbonyls and two asymmetric bridging carbonyls, the latter leaning toward the Pt atoms. The mean plane of the molecule contains Pt(1), Pt(2), P(1), P(2), P(3), C(3), and O(3) (Figure 1). Compared with the coordination sphere about the cobalt center in **4**, that in **7** experiences a tetrahedral distortion with an increase of the angles between the phosphine P(1) or carbonyl C(3)O-(3) and the three carbonyls C(10)O(10), C(20)O(20), C(30)O-(30) or C(1)O(1), C(2)O(2), C(4)O(4), respectively, as shown

(17) *MolEN (Molecular Structure Enraf-Nonius)*; Enraf-Nonius: Delft, The Netherland, 1990.
(18) North, A. C. T.; Philips, D. C.; Mathews, F. S. *Acta Crystallogr., Sect. A.* **1968**, 351.
(19) *International Tables for X-ray Crystallography*, vol IV; Kynoch Press: Birmingham, 1974.
(20) Sheldrick, G. M. *SHELXL 97, Program for the Refinement of Crystal Structures*; University of Göttingen: Germany, 1993.
(21) Hoffmann, R.; Lipscomb, W. N. *J. Chem. Phys.* **1962**, *36*, 2179.
(22) Hoffmann, R.; Lipscomb, W. N. *J. Chem. Phys.* **1962**, *37*, 2872.
(23) Hoffmann, R. *J. Chem. Phys.* **1963**, *39*, 1397.
(24) Ammeter, J. H.; Burgi, H. B.; Thibeault, J. C.; Hoffmann, R. *J. Am. Chem. Soc.* **1978**, *100*, 3686.
(25) Summerville, R. H.; Hoffmann, R. *J. Am. Chem. Soc.* **1976**, *98*, 7240.
(26) Macchi, P.; Proserpio, D. M.; Sironi, A. *Organometallics* **1997**, *16*, 2101.
(27) Mealli, C. *J. Am. Chem. Soc.* **1985**, *107*, 2245.
(28) Archambault, C.; Bender, R.; Braunstein, P.; Bouaoud, S.-E.; Rouag, D.; Golhen, S.; Ouahab, L. *Chem. Commun.* **2001**, 849.
(29) Bender, R.; Braunstein, P.; Fischer, J.; Ricard, L.; Mitschler, A. *New J. Chem.* **1981**, *5*, 81.

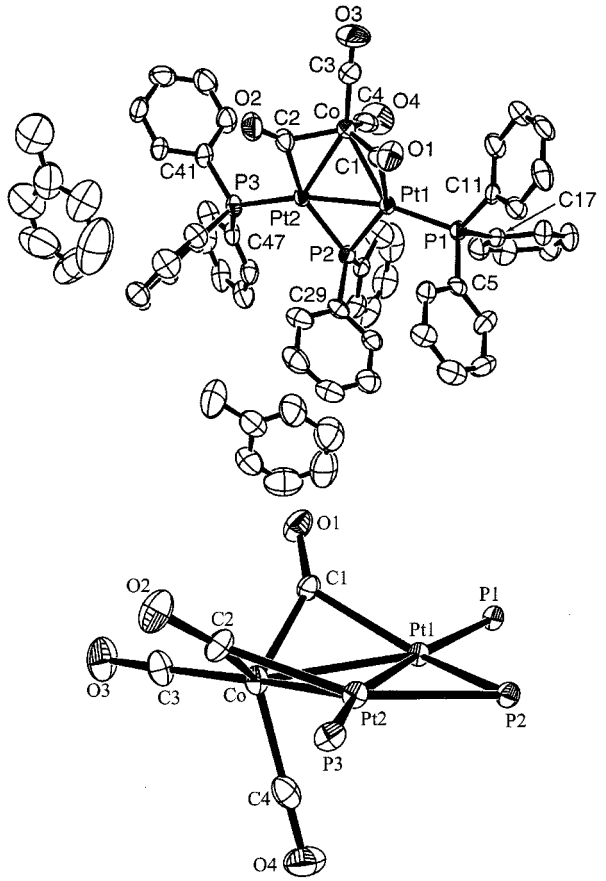

Figure 1. ORTEP view of the structure of $[Pt_2Co(\mu\text{-}PPh_2)(CO)_4(PPh_3)_2]\cdot 2PhMe$ (**7**·2PhMe) (top view) and a side view of the central core (bottom).

Table 2. Selected Bond Distances (Å) and Angles (deg) in $[Pt_2Co(\mu\text{-}PPh_2)(CO)_4(PPh_3)_2]\cdot 2PhMe$ (**7**·2PhMe)

Distances			
Pt(1)−Pt(2)	2.655(1)	Co−C(1)	1.86(1)
Pt(1)−Co	2.547(2)	Co−C(2)	1.86(1)
Pt(2)−Co	2.574(2)	Co−C(3)	1.75(1)
Pt(1)−C(1)	2.083(9)	Co−C(4)	1.82(1)
Pt(1)−P(1)	2.252(2)	C(1)−O(1)	1.15(1)
Pt(1)−P(2)	2.265(2)	C(2)−O(2)	1.14(1)
Pt(2)−P(2)	2.261(2)	C(3)−O(3)	1.14(1)
Pt(2)−P(3)	2.253(2)	C(4)−O(4)	1.14(1)
Pt(2)−C(2)	2.11(1)		

Angles			
C(1)−Pt(1)−P(1)	97.8(3)	C(2)−Pt(2)−P(3)	95.4(3)
P(1)−Pt(1)−Pt(2)	166.28(6)	P(3)−Pt(2)−Pt(1	166.65(7)
P(1)−Pt(1)−P(2)	113.22(9)	P(3)−Pt(2)−P(2)	112.66(9)
C(1)−Pt(1)−Co	46.0(3)	C(2)−Pt(2)−Co	45.6(3)
C(1)−Pt(1)−Pt(2)	92.1(3)	C(2)−Pt(2)−Pt(1)	97.0(3)
P(2)−Pt(1)−Pt(2)	54.0(1)	P(2)−Pt(2)−Pt(1)	54.14(6)
Co−Pt(1)−Pt(2)	59.28(4)	Co−Pt(2)−Pt(1)	58.26(3)
Pt(1)−Co−Pt(2	62.46(4)	Pt(1)−P(2)−Pt(2	71.86(8)
Co−C(1)−O(1)	145.5(8)	Co−C(2)−O(2)	142.9(8)
Pt(1)−C(1)−O(1)	134.0(8)	Pt(2)−C(2)−O(2)	136.5(8)
Co−C(1)−Pt(1)	80.3(4)	Co−C(2)−Pt(2)	80.6(4)
Co−C(3)−O(3)	177.9(11)	Co−C(4)−O(4	179.2(11)
C(1)−Co−Pt(1)	53.7(3)	C(2)−Co−Pt(2)	53.9(3)
C(3)−Co−C(1)	95.1(5)	C(1)−Co−C(2)	107.7(5)
C(3)−Co−C(2)	99.8(5)	C(1)−Co−C(4)	125.0(5)
C(3)−Co−C(4)	104.4(5)	C(2)−Co−C(4)	118.4(5)

in Scheme 2. This corresponds to a geometry of the ligand arrangement somewhat intermediate between that in **5** and **6**.

Scheme 2. Comparison between the Intercarbonyl/Phosphine Bond Angles (in deg) around the Cobalt Center in **4** (Left) and **7** (Right)

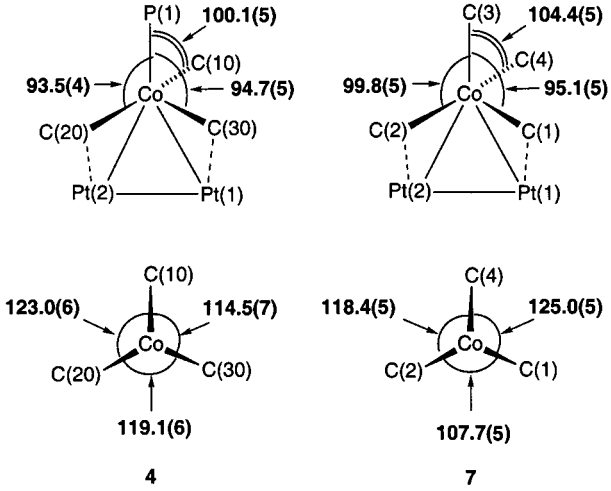

4 **7**

Discussion

The substitution of the terminal chloride in $[Pt_2Cl(\mu\text{-}PPh_2)(PPh_3)_3]$ by the $Co(CO)_4$ group results in the formation of cluster **7** with elimination of NaCl and liberation of PPh_3. This allows the carbonylmetalate to occupy the coordination sites thus liberated and adopt a bridging position on the remaining $Pt_2(\mu\text{-}PPh_2)(PPh_3)_2$ fragment. The distances and angles in the structures of clusters **7** and **4** are very similar, although, when ignoring the metal−metal bonds, the $Co(CO)_4$ fragment experiences a slightly more tetrahedral deformation in **7** compared to the trigonal pyramidal geometry of the $Co(CO)_3(PPh_3)$ fragment a in **4**. The (μ-C)−Co−(μ-C) angles are very similar in both solids (Scheme 2). One could have expected that the steric consequences of the presence of a PPh_3 ligand in **4** include the repulsion of the remaining terminal CO group toward the bridging carbonyls, thus allowing the phosphine ligand to adopt a more symmetrical position on the C_2 axis of the skeleton of **4**. However, this effect is more pronounced in **7** although the steric demand of the carbonyl ligand C(3)O(3) is much lower than that of PPh_3. Electronic effects should therefore also be taken into account. In most structures reported (Cambridge Crystallographic Data Base), the fragments $Co(CO)_4$ and $Co(CO)_3(PR_3)$ occupy terminal positions, but in $[Bi_2Fe_2Co(CO)_{10}]^-$, a $Co(CO)_4$ fragment bridges two Bi atoms, however, without bridging or semibridging carbonyls.[30,31] Three Pd_2Co clusters suggested to contain a $Co(CO)_4$ moiety in bridging position between two mutually bonded Pd atoms have been reported, but only one of them presents an IR spectrum similar to that of **7**. Unfortunately, no crystal structure determination was reported.[32] Clusters **4** and **7** contain two Pt(I) atoms, with the bridging units $Co(CO)_3L$ and PPh_2 being considered as monoanionic. Like the well-

(30) Whitmire, K. H.; Raghuveer, R. S.; Churchill, M. R.; Fettinger, J. C.; See, R. F. *J. Am. Chem. Soc.* **1986**, *108*, 2778.
(31) Whitmire, K. H.; Shieh, M.; Lagrone, C. B.; Robinson, B. H.; Churchill, M. R.; Fettinger, J. C.; See, R. F. *Inorg. Chem.* **1987**, *26*, 2798.
(32) Werner, H.; Thometzek, P.; Kruger, C.; Kraus, H.-J. *Chem. Ber.* **1986**, *119*, 2777.

known 4e donor anionic ligands μ-PPh_2^- and μ-(allyl)$^-$, the $Co(CO)_3L^-$ anion should also be considered here as a 4e donor in order for each Pt atom to reach a 16e count. Theoretical calculations have confirmed that other carbonylmetalates, such as $[(Mo\ or\ W)Cp(CO)_3]^-$, can also be considered as formal 4e donors when they bridge an [m]−[m] hinge ([m] = $Pd(PPh_3)$ or $Pt(PPh_3)$) in structurally related complexes.[33] This allows an isolobal relationship to be established between complexes which all possess a d^9−d^9 unit as [m]−[m] hinge[10,12,15,32,34−39] and helps rationalize the existence of other clusters, like $[Pt_2\{\mu\text{-}MCp(CO)_3\}(\mu\text{-}PPh_2)(PPh_3)_2]$ (M = Mo or W), which has been obtained in the meantime.[28]

MO Analysis. The title clusters **4** and **7** have been analyzed from a EHMO point of view, particularly for the frontier MOs of the model fragments $Co(CO)_4^-$ and $[Pt_2(\mu\text{-}PH_2)(PH_3)_2]^+$. A 4e donor/acceptor model accounting for the interactions between the Lewis base and the d^9−d^9 diplatinum unit implies a suitable symmetry and energy of the MO levels for these fragments. The HOMO and HOMO − 1 for the Co species and LUMO and LUMO + 1 for the Pt_2^+ dimer will be of particular interest and must be examined in more detail.

The tetrahedral (T_d) $Co(CO)_4^-$ anion must strongly distort in **7** in order to allow Pt to approach to Co center and thereby promote Co−Pt bonding. Two limiting distorted geometries are of C_{3v} symmetry with 3 CO groups being coplanar with the cobalt atom and a C_{2v} structure with one of the C−Co−C angle opening up. These C_{3v} and C_{2v} fragments will now be described. The C_{3v} structure reduces steric hindrance and allows more efficient Co···Pt interactions. However, this structure is energetically unfavorable as the computed total EHMO energy moves significantly uphill, by about 1.3 eV relative to the T_d form. The calculated total EHMO energy values are reported in Figure 2. A more important observation is that both T_d and C_{3v} fragments do not exhibit the appropriate MO scheme to allow an overall 4e donor interaction. This is easily deduced from the fact that the ligand field splitting generates the known *e* and t_2 (HOMO) MOs for the tetrahedral anion and two *e* and *a* (HOMO) MOs for the trigonal pyramidal geometry (C_{3v}). For a 4e donor interaction, two nondegenerate MO levels must have the highest energies and appropriate symmetry. Clearly, the M-localized t_2 and $e + a_1$ filled orbitals for the T_d and C_{3v} geometries, respectively, cannot provide the adequate conditions for such a model.

The C_{2v} structure exhibits the five expected nondegenerated filled MO levels, which are of symmetry $b_2 > b_1 > a_1$

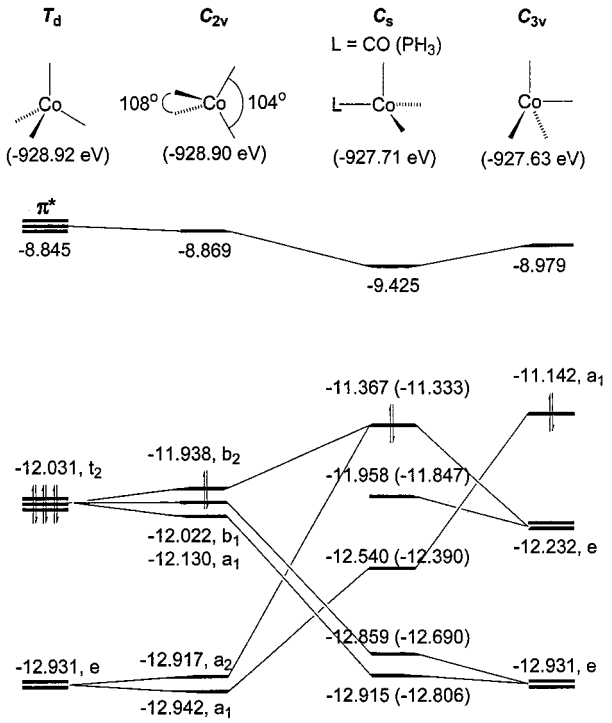

Figure 2. Correlation diagram of the frontier orbitals of the $Co(CO)_4^-$ anion in its T_d, C_{2v}, C_s, and C_{3v} conformations. The $Co(CO)_3(PH_3)^-$ anion (C_s symmetry) is also analyzed, and the MO energies are shown in parentheses beside the $Co(CO)_4^-$ data. For simplicity, the correlation lines address only the major metallic d orbital contributions. The total EHMO energies for each fragment are indicated in brackets under the structures. All ligands are COs except for L where L = CO or PH_3.

> a_2 > a_1. These orbitals are composed primarily of d_{yz}, d_{xz}, d_{xy}, $d_{x^2-y^2}$, and d_{z^2} metal orbitals, respectively, all heavily mixed with π^* MOs of the carbonyl ligands. The total EHMO energy is very sensitive to the C−Co−C angle, for angles exceeding 130° (Supporting Information, Figure S-1). However, between 100° and 120°, the total energy does not vary much, with a minimum at about 110°, as anticipated (i.e., 109.47° for an ideal tetrahedral geometry). According to the X-ray structure, the C−Co−C angles (here defined as C_b−Co−C_b, angle between the two bridging CO ligands, and C_t−Co−C_t, between the two terminal CO ligands) do not deviate strongly from the ideal values (108° and 104°, respectively). The distortion away from the ideal T_d structure of this 108°/104° C_{2v} geometry induces only small atomic and energetic perturbations to the HOMO t_2 orbitals. For instance, upon such a distortion, the total EHMO energy moves up from −928.92 to −928.90 eV, and the t_2 orbitals in the T_d structure (−12.031 eV) barely split into b_2 (−11.938 eV), b_1 (−12.022 eV), and a_1 (−12.130 eV). Similarly, the LUMO (π^*) is also slightly stabilized by 0.02 eV (down to −8.869 eV). This distortion is not very much uphill, which suggests that this could be an easy pathway towards the "preparation" of the $Co(CO)_4^-$ fragment for nucleophilic interactions onto the Lewis Pt_2 acid center. Importantly, the HOMO (b_2; d_{yz}) exhibits the appropriate symmetry to interact with the LUMO of the $[Pt_2(\mu\text{-}PPh_2)(PPh_3)_2]^+$ fragment described below.

The actual conformation of the $Co(CO)_4^-$ in **7** reveals that the C_b−Co−C_b and C_t−Co−C_t C_2 axes are not parallel, but

(33) Hofmann, P.; Schmidt, H. R. *Angew. Chem., Int. Ed. Engl.* **1986**, *25*, 837.
(34) Taylor, N. J.; Chieh, P. C.; Carty, A. J. *J. Chem. Soc., Chem. Commun.* **1975**, 448−449.
(35) Leoni, P.; Pasquali, M.; Fadini, L.; Albinati, A.; Hofmann, P.; Metz, M. *J. Am. Chem. Soc.* **1997**, *119*, 8625−8629.
(36) Vilar, R.; Mingos, D. M. P.; Cardin, C. J. *J. Chem. Soc., Dalton Trans.* **1996**, 4313−4314.
(37) Dura-Vila, V.; Mingos, D. M. P.; Vilar, R.; White, A. J. P.; Williams, D. J. *J. Organomet. Chem.* **2000**, *600*, 198−205.
(38) Werner, H.; Kühn, A. *J. Organomet. Chem.* **1979**, *179*, 439.
(39) Werner, H.; Kraus, H.-J. *Chem. Ber.* **1980**, *113*, 1072.

somewhat tilted. The two C_b-Co-C_b and C_t-Co-C_t planes remain perpendicular to each other, indicating that the C_s distortion proceeds via a slight sliding motion of these triangular planes. The produced distortion leads to a C_s symmetry which induces an even more important ligand field splitting with the expected five nondegenerate MO levels in comparison with the C_{2v} structure. With this geometry, the 4e donor interaction proposal becomes readily more plausible.

The correlation diagram between the four described forms (T_d, C_s, C_{2v}, and C_{3v}) is shown in Figure 2. The total EHMO energy for the C_s symmetry is close to that computed for the C_{3v} structure, indicating that the C_s deformation is energetically as demanding as the C_{3v} one. The HOMO energy varies as $T_d \sim C_{2v} < C_s \sim C_{3v}$, somewhat following the total EHMO energy. The HOMO − 1 level for the C_s geometry is also slightly destabilized, being energetically higher than the t_2 and e levels in the T_d and C_{3v} geometries, respectively. This observation also argues in favor of the 4e model.

The MO diagram for the $Co(CO)_3(PH_3)^-$ fragment in relation with compound **4** was also analyzed for comparison. The MO scheme is essentially identical to that of $Co(CO)_4^-$ with minor variations of the MO energies (Figure 2). The conclusions drawn from calculations for the $Co(CO)_4^-$ fragment are strongly anticipated to be the same for this derivative, and it was not investigated further in this work. The LUMO in all four computed geometries are localized within the π^*(CO) systems. For the C_s geometry, this LUMO is more significantly stabilized than in the other structures (with T_d, C_{2v}, and C_{3v} geometries), suggesting that the C_s structure energetically favors back-bonding interactions. The atomic contributions of the HOMO in the C_s geometry (Supporting Information, Table S-1) indicate a very large Co metal composition (about $^2/_3$) and a minor but still significant contribution from the CO residues (about $^1/_3$). The combination of the $d_{x^2-y^2}$ (34%) and p_y (15%) Co orbitals generates an orbital exhibiting a large lobe pointing along the y axis of the $Co(CO)_4^-$ fragment, exactly where Co···Pt interactions occur. In addition, three of the four CO ligands contribute to this HOMO using their π^* systems via positive overlaps between the Co and the carbon atoms of these carbonyls. This observation is important because it takes into account the possibility of favorable symmetry interactions between the Co, the bridging carbonyls, and the Pt centers. The HOMO − 1 does not show a large lobe for interactions but rather exhibits two lobes of opposite signs issued from a distorted butterfly-shaped MO, hence providing an opportunity for antisymmetric interactions.

The Lewis acid model fragment $Pt_2(\mu\text{-}PH_2)(PH_3)_2^+$ can be described as a C_{2v} planar moiety. Prior to letting this A-frame acid interact with the Lewis base $Co(CO)_4^-$ (C_s), one can easily anticipate a change in the P−Pt−P angle, from a configuration with a larger and more sterically demanding angle, to a smaller one, allowing the $Co(CO)_4^-$ moiety to efficiently interact with the metal Pt centers. The total EHMO energies of the $[Pt_2(\mu\text{-}PH_2)(PH_3)_2]^+$ fragment as a function of the P−Pt−P angle (the dinuclear species was kept in a C_{2v} point group) were computed (Figure 3). Two energy minima were detected corresponding to angles of 149° (most stable) and 188°. The presence of these minima is easy to rationalize. The two-electron donor PH_3 ligands tend to occupy vacant sites for Pt−P bonding with best possible overlaps. Because of bonding in the $Pt_2(\mu\text{-}PH_2)$ fragment, the atomic contributions are set to adjust for the triangular shape. As a consequence in the LUMO and HOMO, the in-plane Pt orbitals exhibit deformed butterfly d-shaped lobes pointing somewhat in the opposite direction to the Pt−Pt and Pt−P bonds. The unsaturated sites at the Pt atoms are then oriented slightly off linearity of the Pt−Pt and Pt−P bonds, in fact, forming $Pt-Pt-PH_3$ and $H_2P-Pt-PH_3$ angles of about 185° and 188°, respectively. The computed barriers between the two forms are relatively small: 0.082 (660) and 0.056 eV (450 cm^{-1}), and one may anticipate motions in the gas phase. The energy potential walls at lower and higher angles are explained by poorer orbital overlaps between the Pt and PH_3 ligands and steric hindrance between the H atoms of the PH_3 groups, respectively. This latter behavior is translated by a steeper slope of the potential wall. The lowest energy configuration (149°) exhibits sufficient space for an approach of the $Co(CO)_4^-$ anion toward the Pt_2 moiety, including the presence of the larger Ph groups in the space filling model for the fragment $[Pt_2(\mu\text{-}PPh_2)(PPh_3)_2]^+$ (Supporting Information, Figure S-2). The experimental P−Pt−P angle is about 112.5° and is located uphill (by +0.87 eV) with respect to the minimum energy form. The atomic contributions in the dinuclear Pt fragment (Supporting Information) exhibit well isolated LUMO (b_2) and LUMO

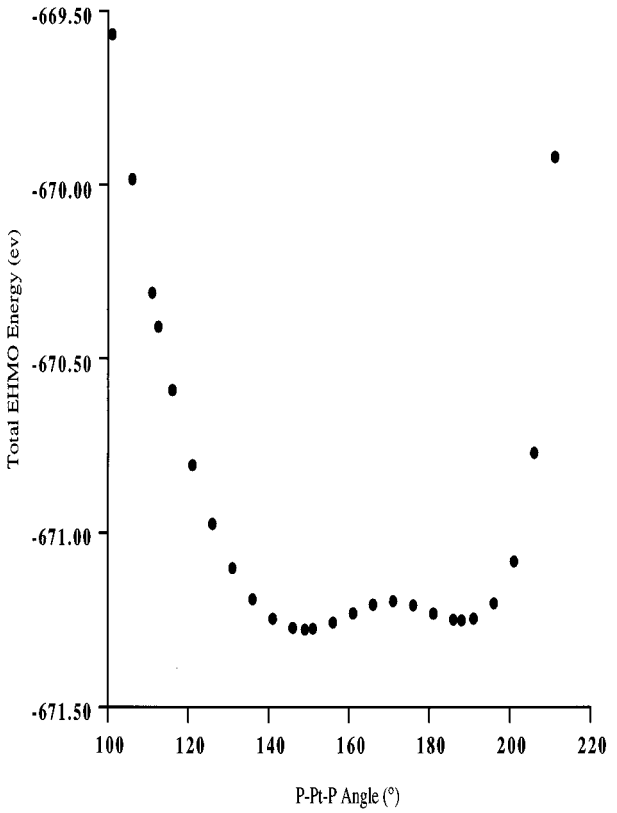

Figure 3. Plot of the total EHMO energy of the $[Pt_2(\mu\text{-}PH_2)(PH_3)_2]^+$ fragment as a function of the P−Pt−P angle.

Table 3. Atomic Contributions of the $CoPt_2(\mu\text{-}PH_2)(PH_3)_2(CO)_4$ Model Compound for Selected Frontier MOs[a]

MO	energy (eV)	Pt						Co						C			P		
		d_{z^2}	$d_{x^2-y^2}$	d_{xy}	d_{xz}	d_{yz}	others	d_{z^2}	$d_{x^2-y^2}$	d_{xy}	d_{xz}	d_{yz}	others	p_x	p_y	p_z	p_x	p_y	p_z
LUMO + 1[b]	−9.217	4		4			10(p_y)				6			26	18	11	9	4	
LUMO	−10.072	32	6				4(p_z)				4	3	4(p_z)			23			3
HOMO[c]	−11.075			4	14		12(p_x)	12	10	3			3(p_x)	15			6		
HOMO − 1	−11.896		6	20		20		18	5	16			3(p_z)		8	6		2	
HOMO − 2	−12.047	4	6		18						28	19	4(p_z)			7			5
HOMO − 3	−12.215	18	14	20		4	4(p_z)	13	2	10									

[a] Contributions less than 1% are not included. The C_2 axis is the x axis, and the M and P atoms are in the xy plane. [b] This MO also contains 2% of P(p_z) contributions (lone pairs). [c] This MO also contains 3% μ-P (p_x) contributions (lone pairs).

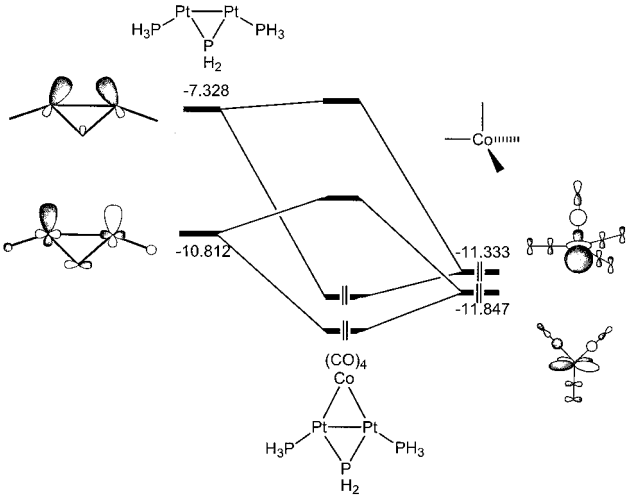

Figure 4. Simplified MO diagram showing the 4e interactions between the $Co(CO)_4^-$ (HOMO and HOMO − 1) and $[Pt_2(\mu\text{-}PH_2)(PH_3)_2]^+$ fragments (LUMO and LUMO + 1). In this diagram, there are no bridging COs.

+ 1 (a_1). The LUMO is composed primarily of in-plane Pt atomic orbitals. The major contributors to this MO are the d_{z^2} and $d_{x^2-y^2}$ atomic orbitals generating larger lobes of opposite signs pointing slightly off the *z*-axis (for subsequent Pt−Co bondings). Within this fragment, the Pt−Pt and Pt−P interactions are all antibonding. The LUMO + 1 is also of Pt origin but is composed exclusively of in-plane p and s orbitals. These results are consistent with the electronic configuration of the Pt_2 center (d^9-d^9). As a consequence, the MO energy for this LUMO + 1 is high.

The symmetry of the LUMO and LUMO + 1 of the Pt_2 fragment (Figure 4) is appropriate for interactions with the HOMO − 1 and HOMO of $Co(CO)_4^-$ (both in the C_s and C_{2v} forms), respectively. The EHMO energy difference between the LUMO of the Pt_2 fragment (−10.812 eV) and the HOMO − 1 of the Co moiety (−11.847 eV) is relatively small and adequate for efficient interactions. Conversely, the LUMO + 1 of the Pt_2 residue is relatively destabilized for the reason mentioned above, and the energy difference with the $Co(CO)_4^-$ HOMO is, as expected, large (about 4 eV). Therefore, this second bonding provides much less stabilization according to this model (Figure 4). Such interactions do indeed occur with the predicted effects.

At this stage, the MO picture is, in fact, incomplete without the contributions of the bridging carbonyls. By adding the bridging interaction of two of the COs as in the final product, some additional stabilization is provided, and the frontier orbitals become heavily mixed. Details of the atomic contributions are provided in Table 3. This analysis focused mainly on M−M′ bonding because in a general sense 4e donor fragments do not always contain bridging COs. Metal−metal bonding interactions are still the main driving forces for cluster formation. Of particular interest is that the LUMO + 1 exhibits little Co metal contributions as anticipated by the large gap discussed previously but finds additional stabilization by using CO atomic contibutions via the π^* systems. This second observation agrees with predictions made above for the lower energy π^* orbitals of the $Co(CO)_4^-$ fragment (C_s symmetry). As a consequence, this MO exhibits a large contribution from the bridging carbonyls. It is believed, although this was not investigated in this work, that bridging the two COs induces a change in P−Pt−P angle toward the observed 112.5 °, owing to electronic, but also obvious steric Ph···CO reasons.

Conclusion

The new cluster $[Pt_2Co(\mu\text{-}PPh_2)(CO)_4(PPh_3)_2]$, **7**, has been synthesized and characterized crystallographically. It consists of a d^9-d^9 $Ph_3P \rightarrow Pt(I)-Pt(I) \leftarrow PPh_3$ metal−metal bonded unit bridged by two monoanionic fragments, PPh_2^- and $Co(CO)_4^-$. The EHMO analysis is consistent with the proposed description of the 18e metal carbonyl fragment acting as an anionic 4e donor. The d^9-d^9 electronic configuration of the Pt_2 moiety makes the energy of its LUMO + 1 unavoidably high, leading to a minor contribution to the stabilization of the clusters. However, additional stabilization occurs when bridging carbonyls participate in the binding of the two fragments (Pt_2 + Co). It can be anticipated that the number of organometallic fragments that will be characterized in the future as 4e donors in metal clusters will be growing.[40]

Acknowledgment. We thank the Centre National de la Recherche Scientifique, the Ministère de la Recherche, the Ministère des Affaires Etrangères (Paris), and the Ministère des Affaires Etrangères (Alger) for support of the Strasbourg-Constantine Cooperation Project 96 MDU 371. This project was also supported by the Fonds International de Coopération Universitaire-FICU (AUPELF-UREF, Agence Universitaire de la Francophonie).

Supporting Information Available: Tables giving details of the structure determination, atomic coordinates including those of the hydrogen atom, anisotropic thermal parameters, and bond

(40) Braunstein, P.; Oro, L. A.; Raithby, P. R. *Metal Clusters in Chemistry*; Wiley-VCH: Weinheim, 1999.

lengths in CIF format. Plots of the total EHMO energy of the $Co(CO)_4^-$ anion during a C_{2v} distortion about the opening of one of the C−Co−C angles (Figure S-1), and space filling model of the $[Pt_2(\mu\text{-}PPh_2)(PPh_3)_2]^+$ fragment in the lowest energy conformation (P−Pt−P angle, ∼150 °) (Figure S-2). Tables giving the atomic contributions of the $Co(CO)_4^-$ anion in the C_s geometry (Table S-1) and the $[Pt_2(\mu\text{-}PPh_2)(PPh_3)_2]^+$ fragment (Tables S-2) for selected frontier MOs. This material is available free of charge via the Internet at http://pubs.acs.org.

IC010739P